DocuServe

Electronic Delivery Cover Sheet

Caltech Library Services

Received: 12 October 2020 | Revised: 1 April 2021 | Accepted: 6 April 2021

DOI: 10.1111/ter.12531

RESEARCH ARTICLE

Terra Nova WILEY

Emergence of continents above sea-level influences sediment melt composition

Janne Liebmann[1] | Christopher J. Spencer[2,3] | Christopher L. Kirkland[1] | Claire E. Bucholz[4] | Xiao-Fang He[5] | M. Santosh[6,7] | Xiaoping P. Xia[8] | Laure Martin[9] | Noreen J. Evans[10]

[1]Timescales of Mineral Systems Group, The Institute for Geoscience Research (TIGeR), School of Earth and Planetary Sciences, Curtin University, Perth, Western Australia, Australia

[2]Department of Geological Sciences and Geological Engineering, Queen's University, Kingston, Ontario, Canada

[3]The Institute for Geoscience Research (TIGeR), School of Earth and Planetary Sciences, Curtin University, Perth, Western Australia, Australia

[4]Division of Geological and Planetary Sciences, California Institute of Technology, Pasadena, California, USA

[5]School of Geoscience and Surveying Engineering, China University of Mining & Technology, Beijing, China

[6]China University of Geosciences, Beijing, China

[7]Department of Earth Sciences, University of Adelaide, Adelaide, South Australia, Australia

[8]State Key Laboratory of Isotope Geochemistry, Guangzhou Institute of Geochemistry, Chinese Academy of Sciences, Guangzhou, China

[9]Centre for Microscopy, Characterisation, and Analysis, ARC Centre of Excellence for Core to Crust Fluid Systems (CCFS), University of Western Australia, Perth, Western Australia, Australia

[10]School of Earth and Planetary Science, John de Laeter Centre, Curtin University, Perth, Western Australia, Australia

Correspondence
Janne Liebmann, School of Earth and Planetary Sciences, The Institute for Geoscience Research (TIGeR), Curtin University, Perth, Western Australia, Australia.
Email: janne.liebmann@curtin.edu.au

Funding information
The University of Western Australia; Australian Government; Australian Education Investment Fund program; Australian Research Council LIEF program

Abstract

The Archean-Proterozoic transition heralded a number of fundamental changes on Earth, including the oxygenation of the atmosphere, a marked emergence of continents above sea-level, and an increase in $\delta^{18}O$ of felsic magmas. The potential drivers for the latter are changes in the composition of supracrustal material or increased crustal reworking. Although the onset of subduction-induced continental collision and associated enhanced crustal recycling could produce high-$\delta^{18}O$ felsic magmas, temporally constrained zircon $\delta^{18}O$ reveals an increase in $\delta^{18}O$ at ~2.35 Ga that predates the oldest widely recognized supercontinent. In this work, we use the O and Hf isotope ratios of magmatic zircon crystals in Archean and Proterozoic sediment-derived granitoids of the North China Craton to track the incorporation of supracrustal material into magmas. The results are consistent with a Paleoproterozoic increase of continental freeboard producing sedimentary reservoirs with comparatively elevated $\delta^{18}O$ that subsequently partially melted to generate the granitoids.

1 | INTRODUCTION

In the past two decades, a number of works have discussed the secular evolution of O isotopes in zircon (Kirkland et al., 2010; Payne et al., 2015; Spencer et al., 2014; Valley et al., 2005). The O isotope ratio ($^{18}O/^{16}O$) of a melt is sensitive to the incorporation of supracrustal material (Valley et al., 1994). Zircon preserves the most robust record of the O isotopic composition of its parental magma due to its slow O diffusion rate (Valley et al., 1994). Igneous zircon in high-temperature equilibrium with the mantle has homogenous $\delta^{18}O$ values averaging $5.3 \pm 0.6‰$ (Page et al., 2007). Supracrustal material, in contrast, has a wide range of $\delta^{18}O$ values with most reservoirs being elevated in $\delta^{18}O$ relative to the mantle (Eiler, 2001). Hence, assimilation of supracrustal material generally results in magmatic zircon

with higher $\delta^{18}O$ relative to zircon in equilibrium with the mantle. Archean zircon has uniform $\delta^{18}O$ values averaging 5.8 ± 1.0‰ (1σ, n = 2,644), whereas post-Archean zircon $\delta^{18}O$ is more variable and on average higher (6.8 ± 1.8‰; 1σ, n = 13,314) (Spencer et al., 2014; Valley et al., 2005). Statistical change-point analysis of 2.8–1.9 Ga detrital zircon data (n = 452) suggest that the initial rise in average zircon $\delta^{18}O$ occurred at ~2.35 Ga (Spencer et al., 2019). One way to achieve higher $\delta^{18}O$ felsic magmas is through enhanced assimilation of supracrustal material (Kirkland et al., 2010; Spencer et al., 2014) driven by a change in the geodynamic regime (i.e. the onset of subduction-driven collisional tectonics) at the Archean-Proterozoic transition (Condie, 2018; O'Neill et al., 2016). Importantly, however, the initial rise in average zircon $\delta^{18}O$ predates the ~1.9–1.8 Ga assembly of Earth's first widely accepted supercontinent, Nuna (Bleeker, 2003). Instead, the rise in average zircon $\delta^{18}O$ occurred in a period characterized by a global lull in tectono-magmatic activity (Condie et al., 2009; Spencer et al., 2018). Alternatively, increased $\delta^{18}O$ of recycled material (Payne et al., 2015; Valley et al., 2005) could have driven the increase in zircon $\delta^{18}O$ without requiring more efficient recycling. The ~2.35 Ga shift in average zircon $\delta^{18}O$ coincides with the oxygenation of the Earth's atmosphere (Great Oxygenation Event; GOE) (Gumsley et al., 2017; Luo et al., 2016) and an increase in continental freeboard (the average elevation of continental crust above sea-level) (Flament et al., 2013; Hollis et al., 2014) that is proposed to have led to a shift in the triple-oxygen isotope composition of shales (Bindeman et al., 2018).

A model involving crustal reworking has been invoked to explain the rise of average zircon $\delta^{18}O$ at ~2.35 Ga (Spencer et al., 2019). However, this explanation is based on detrital zircon that provides only limited information on the original source-rock given the inherent lack of contextual information, which may only partly be accessible through zircon chemistry (Hawkesworth & Kemp, 2006). In contrast, zircon from sediment-derived melts provide a clear link to the $\delta^{18}O$ of their sedimentary source-rocks. Existing bulk-rock and zircon $\delta^{18}O$ from sediment-derived granites show an increase across the Archean-Proterozoic transition (Bucholz & Spencer, 2019). However, the existing geochemical datasets for Precambrian sediment-derived granitoids are limited in size, particularly, for the critical age span of 2.6–1.8 Ga. This study utilizes zircon O and Hf isotope geochemistry, combined with bulk-rock trace element compositions of Archean to Paleoproterozoic sediment-derived granitoids of the North China Craton (NCC; Figure 1) to further characterize the zircon $\delta^{18}O$ record of sediment-derived melts across this critical transition in Earth history. Samples derive from five geological units in an area extending 300 km E-W and 80 km N-S (Table 1; Appendix A). The isotopic signatures in igneous zircon in combination with protolith information provide a high fidelity record of potential tectonic and compositional drivers for the Paleoproterozoic increase in zircon $\delta^{18}O$.

2 | METHODS

Zircon was isolated using standard density and magnetic separation techniques, and hand-picked grains were mounted in epoxy. Cathodoluminescence (CL) images of zircon grains were taken to reveal internal growth structures. Oxygen isotope analysis was conducted on a CAMECA IMS-1280 secondary ion mass spectrometer (SIMS). Oxygen isotope compositions are reported in the conventional delta notation; expressed as $\delta^{18}O$, the permil deviation of $^{18}O/^{16}O_{sample}$ relative to standard mean ocean water (VSMOW) (Baertschi, 1976; Craig, 1961). The reported zircon $\delta^{18}O$ for each sample are weighted means ±2σ uncertainty. Following O isotope analysis, zircon U-Pb ages were obtained using an A.S.I. SHRIMP II sensitive high-resolution ion microprobe. Hafnium isotopes were analysed via laser ablation inductively coupled plasma mass spectrometry (LA-ICPMS). Unless indicated otherwise, spots of U-Pb, O and Hf isotope analyses were located in the same zircon growth zone (Figure 2). To avoid signatures from inherited growth zones, only analyses located on magmatic rims of zircon grains were used to determine crystallization age, O and Hf isotopic composition of

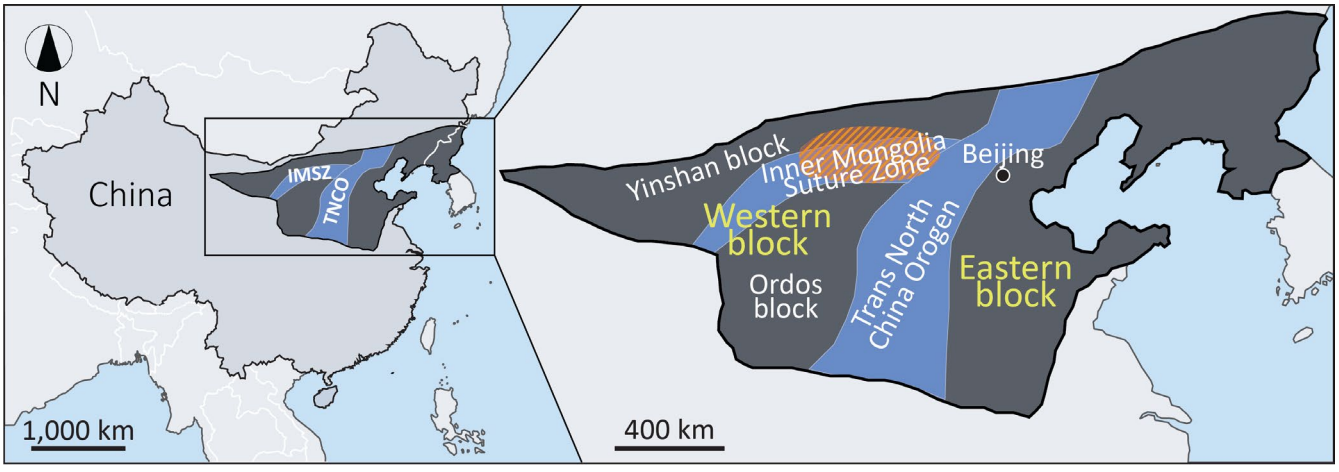

FIGURE 1 Simplified map of the North China Craton (shown in dark grey). Shaded area indicates area of sample collection. See Table 1 for latitude and longitude and supplementary Figure A7 for a more detailed map

TABLE 1 Geological unit, location, lithology, mineralogy, magmatic crystallization ages and zircon $\delta^{18}O$ of samples studied here

Sample ID	Geologic unit	Latitude	Longitude	Rock type	Mineralogy	Age ± 2σ (Ma)	Zircon $\delta^{18}O \pm 2\sigma$ ($‰_{SMOW}$)	Zircon $\delta^{18}O$ *n*
18IM11B	Jining Complex, IMSZ	40.604	112.500	Grt granitoid	Pl+Afs+Qz+Grt+Bt	1901 ± 17	10.80 ± 0.90[b]	8
18IM12B	Jining Complex, IMSZ	40.839	112.565	Grt quartz rich granitoid	Qz+Pl+Afs+Grt	1929 ± 29	9.74 ± 1.16[b]	18
18IM13C	Xiwulanbulang area, YB	41.084	110.924	Grt granite	Qz+Afs+Pl+Grt+Bt(+Ms)	2,536 ± 13	8.12 ± 0.70[c]	18
18IM14A	Daqingshan-Wulashan Complex, IMSZ	40.922	110.961	Grt granite	Qz+Afs+Pl+Bt(+Grt)	1948 ± 72[a]	4.65 ± 0.85[c]	17
18IM15B	Xiwulanbulang area, YB	40.994	110.947	Grt granitoid	Qz+Pl+Afs+Grt	2,530 ± 60	8.75 ± 0.42[c]	11
18IM19	Daqingshan-Wulashan Complex, IMSZ	40.693	109.641	Grt granite	Afs+Qz+Pl+Grt+Bt	2,478 ± 18	7.21 ± 0.58[c]	35
18IM20	Daqingshan-Wulashan Complex, IMSZ	40.709	109.643	Grt granitoid	Qz+Pl+Afs+Grt+Bt	2,374 ± 48[a]	7.39 ± 0.70[b]	17
18IM21C	Daqingshan-Wulashan Complex, IMSZ	40.698	109.721	Grt quartz rich granite	Qz+Afs+Pl+Grt+Bt	1855 ± 16	6.71 ± 0.52[b]	21
18IM23D	Daqingshan-Wulashan Complex, IMSZ	40.811	110.258	Grt granite	Qz+Afs+Pl+Grt	2,453 ± 11	6.31 ± 0.63[b]	13
18IM25C	Guyang area, YB	41.182	109.479	Ms Bt granite	Qz+Afs+Pl+Ms(+Bt)	2,493 ± 28	6.86 ± 0.89[c]	20
18IM3	Huaian Complex, TNCO	40.848	113.921	Grt granite	Qz+Afs+Pl+Grt+Ms(+Bt)	1917 ± 70	11.41 ± 1.00[b]	8

Note: Abbreviations: Afs, alkali feldspar; Grt, garnet; Ms, muscovite, Bt, biotite; Pl, plagioclase; Qtz, quartz.

[a]Weighted mean ages calculated from the oldest statistical coherent population (see Appendix A for a detailed discussion of the U-Pb zircon geochronological data). Minerals are listed from most abundant to least. Minerals in parentheses are accessory phases.

[b]Zircon O isotope analyses were conducted at Guangzhou Institute of Geochemistry, Chinese Academy of Sciences.

[c]Zircon O isotope analyses were conducted at Centre for Microscopy, Characterization and Analysis at the University of Western Australia; *n* indicates number of single grain analyses per sample.

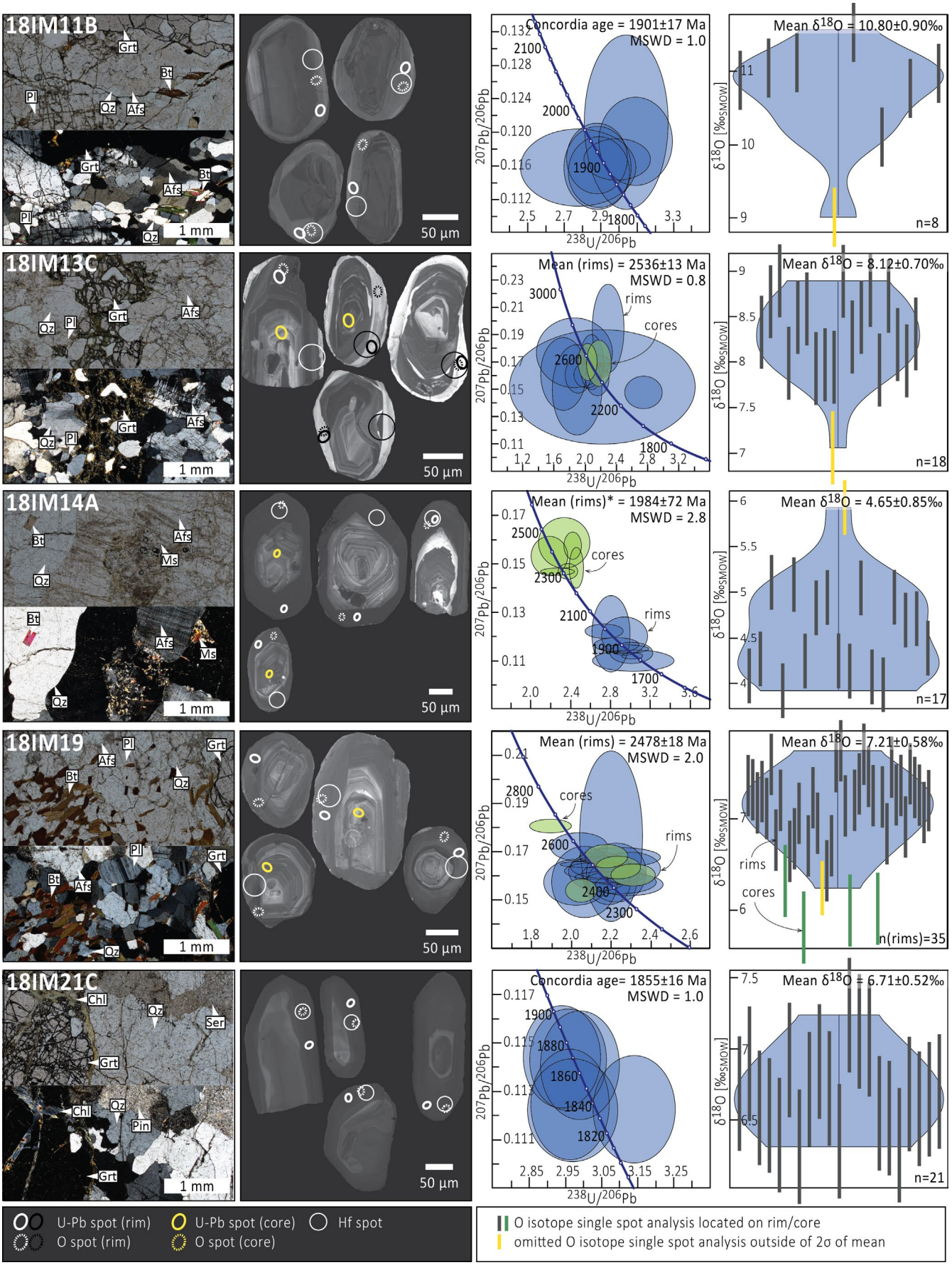
18IM11B
Grt
Bt
Pl
Qz
Afs
1 mm
50 µm
Concordia age = 1901±17 Ma
MSWD = 1.0
Mean δ18O = 10.80±0.90‰
n=8
18IM13C
Mean (rims) = 2536±13 Ma
MSWD = 0.8
rims
cores
Mean δ18O = 8.12±0.70‰
n=18
18IM14A
Ms
Mean (rims)* = 1984±72 Ma
MSWD = 2.8
Mean δ18O = 4.65±0.85‰
n=17
18IM19
Mean (rims) = 2478±18 Ma
MSWD = 2.0
Mean δ18O = 7.21±0.58‰
n(rims)=35
18IM21C
Chl
Ser
Pin
Concordia age= 1855±16 Ma
MSWD = 1.0
Mean δ18O = 6.71±0.52‰
n=21
207Pb/206Pb
238U/206Pb
δ18O [‰SMOW]
U-Pb spot (rim)
U-Pb spot (core)
Hf spot
O spot (rim)
O spot (core)
O isotope single spot analysis located on rim/core
omitted O isotope single spot analysis outside of 2σ of mean

FIGURE 2 Thin section photomicrographs, CL images of representative zircon grains, concordia diagrams and O isotope violin plots of representative samples (see supplementary Figure A1-A3 for complete sample set). Violin plots are hybrids of box plots and probability density curves (Hintze & Nelson, 1998). Spot locations of O, U-Pb and Hf isotope analyses are marked in the CL images. Results of U-Pb analyses on zircon rims and cores are shown as blue and green ellipses, respectively, in concordia diagrams. Concordia ages, weighted mean ages and weighted mean $\delta^{18}O$ (weighted by uncertainty of individual analyses) are quoted with 2σ uncertainty. Quoted weighted mean ages are calculated from most concordant single spot $^{207}Pb/^{206}Pb^*$ ages. Weighted mean age marked with asterisk is calculated from the oldest statistical coherent population. See Appendix A for details of data analysis. Mineral abbreviations: Qz, quartz; Afs, alkali feldspar; Pl, plagioclase; Grt, garnet; Ms, muscovite, Bt, biotite; Ser, sericite; Chl, chlorite

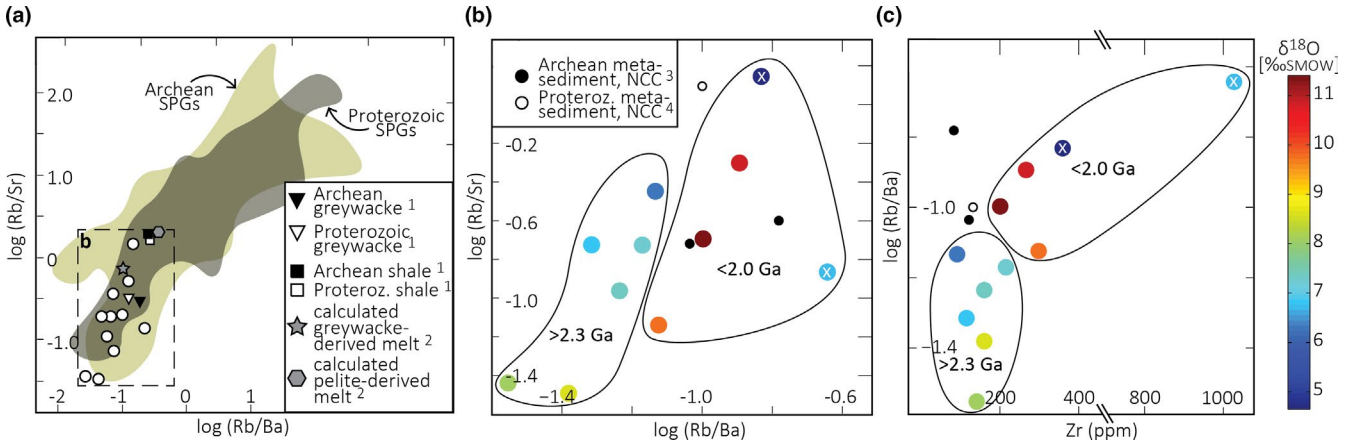

FIGURE 3 (a) Rb/Ba versus Rb/Sr ratios of sediment-derived granitoids of this study (white circles) and Archean and Proterozoic strongly peraluminous granites (SPGs) from Bucholz and Spencer (2019) (Archean SPGs $n = 255$, Proterozoic SPGs $n = 586$). Average compositions of Archean and Proterozoic greywacke and shales are from [1]Condie (1993); compositions of calculated greywacke and pelite-derived melt are from [2]Sylvester (1998). Neither sediment-derived melts nor sediments show a systematic change in Rb/Ba or Rb/Sr ratio across the Archean-Proterozoic transition. Dashed rectangle marks section shown in (b). (b) Rb/Ba versus Rb/Sr ratios, colour-coded by their corresponding zircon $\delta^{18}O$ values. Rb/Ba and Rb/Sr ratios show no correlation with $\delta^{18}O$. Sediment-derived granitoids younger than 2.0 Ga show higher Rb/Ba ratios than their older counterparts (see section 4.3 for discussion). White X marks omitted samples whose bulk-rock composition may be affected by secondary processes (discussed in Appendix A2.4). Compositions of Archean and Proterozoic metasediments in the Yinshan block and Inner Mongolia Suture Zone, respectively, are from [3]Wang & Guo (2017) and [4]Wan et al. (2018). (c) Rb/Ba ratio versus Zr concentration, colour-coded by their corresponding zircon $\delta^{18}O$ values. Higher Rb/Ba ratios in ≤2.0 Ga samples compared to ≥2.3 Ga samples, are associated with higher Zr concentrations. Black and white circles show compositions of metasedimentary rocks in the sampling area potentially reflecting the composition of the source of the sediment-melts of this study (refer to caption and legend of (A) for references and explanation of symbols). There is no evidence for distinct Zr concentrations of the source of the samples studied here, implying that the small differences in Rb/Ba ratios and Zr concentration of these samples may be caused by variable melting temperatures rather than variable composition of the source (discussed in Appendix A2.3); thus, further supporting that no systematic change in the clay-content of the source occurred.

zircon in equilibrium with the melt. Bulk-rock major and trace element concentrations were determined using an X-ray fluorescence spectrometer. A detailed description of the methodology is provided in Appendix A.

3 | RESULTS

The 11 samples studied here include granitoids comprised of quartz, alkali feldspar, plagioclase, garnet, muscovite and biotite in varying proportions. Magmatic crystallization ages of the granitoids range from 2,536 ± 13 Ma to 1855 ± 10 Ma (Table 1). All samples are strongly peraluminous with an aluminium saturation index (ASI)≥1.1 (defined as molar Al/[Ca-1.67P+Na+K]; Supplementary Table D1) and contain at least one aluminous mineral, such as garnet or muscovite. Strongly peraluminous granitoids are generally interpreted to have formed through the partial melting of (meta-) sedimentary rocks (Chappell & White, 1992; Frost & Frost, 2008). Hence, both mineralogy and geochemistry of all samples support the derivation from sedimentary protoliths, in accord with previous petrogenetic interpretations (Dan et al., 2012; Zhao et al., 1999). All samples show Rb/Sr and Rb/Ba ratios below 1.5 and 0.5 respectively (Supplementary Table D1). Samples with crystallization ages <2.0 Ga show Rb/Ba ratios of 0.08–0.15 similar to those of samples >2.3 Ga with Rb/Ba ratios of 0.03–0.07. The Rb/Sr ratios of both groups are indistinguishable ranging from 0.03–1.4 (Figure 3).

With the exception of sample 18IM14A, the NCC granites yield zircon $\delta^{18}O$ higher than the mantle value of 5.3 ± 0.6‰ (Page et al., 2007), as expected for rocks with sedimentary sources (Valley et al., 1994). Based on the timing of the increase in average $\delta^{18}O$ in detrital zircon at 2.35 Ga (Spencer et al., 2019),

the granitoids of this study are grouped according to their magmatic crystallization age. Zircon from sediment-derived granitoids with crystallization ages >2.3 Ga yield $\delta^{18}O$ of 6.9 ± 0.9‰ to 8.6 ± 0.4‰ (Table 1). Sediment-derived granitoids with crystallization ages <2.0 Ga have a wider range of zircon $\delta^{18}O$ from 4.7 ± 0.9‰ to 11.4 ± 1.0‰, but on average have higher $\delta^{18}O$ than older samples (Figure 4).

Zircon $\delta^{18}O$ is typically interpreted in tandem with εHf (deviation of $^{176}Hf/^{177}Hf$ in parts per 10,000 from the chondritic uniform reservoir), as elevated $\delta^{18}O$ is often linked to enhanced crustal reworking and evolved Hf isotopic signatures (low εHf) (Hawkesworth & Kemp, 2006). The vast majority of single grain analyses yield εHf values between −10 and +15 (Figure 5). Of the 154 analyses, only two single grain analyses of sample 18IM3 show εHf values <−10. There is no correlation between higher $\delta^{18}O$ and evolved εHf values.

Detailed results of individual samples are provided in Appendix A and in supplementary Tables B1, C1 and D1.

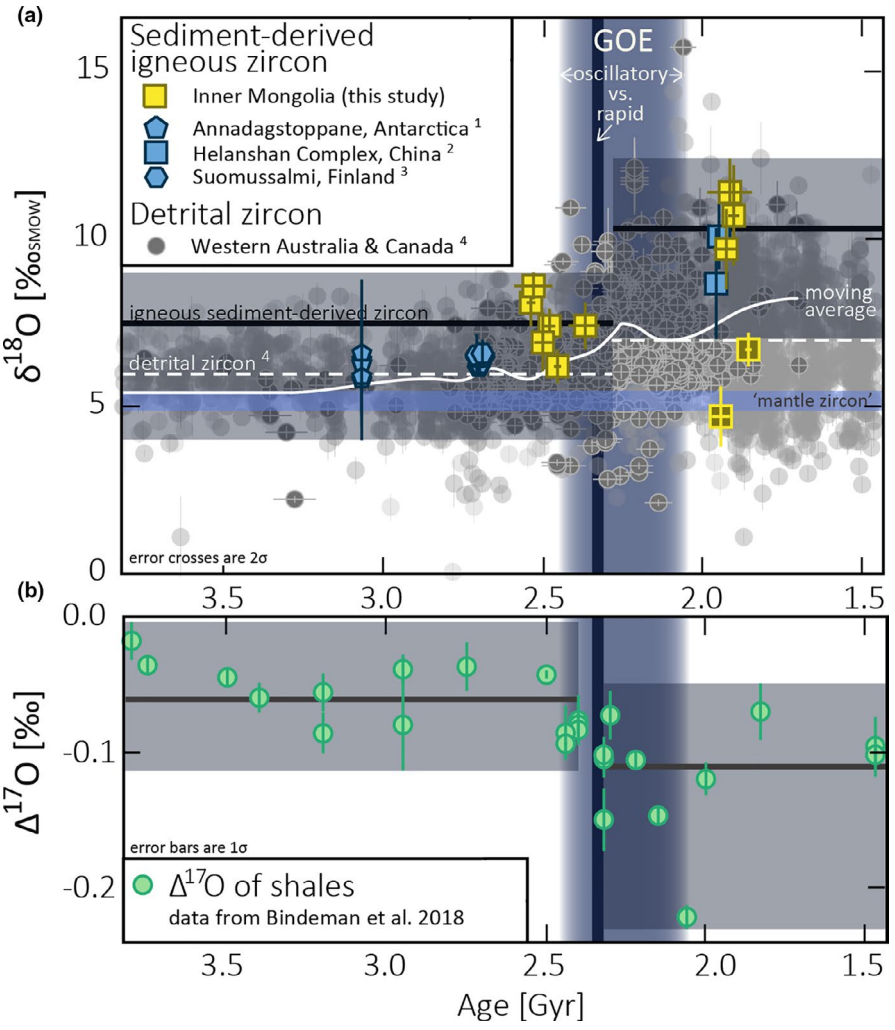

FIGURE 4 (a) Variation in zircon $\delta^{18}O$ with >1.5 Ga crystallization ages. Yellow symbols show data of sediment-derived igneous zircon from this study. Blue symbols refer to zircon data from strongly peraluminous granites from [1]Marschall et al. (2010), [2]Dan et al. (2014), and [3]Mikkola et al. (2011). Opaque grey symbols show data of detrital zircon from Spencer et al. (2019). Transparent grey symbols show compiled global zircon $\delta^{18}O$ data from Spencer et al. (2017). Both detrital zircon and igneous zircon from sediment-derived melts show a shift in average O isotope composition before and after ~2.35 Ga, as indicated by solid black and dashed white line, respectively. The ~3.5‰ shift in average zircon $\delta^{18}O$ of the sediment-derived granitoids of this study is more prominent than the deviation of 1.1‰ shown by detrital zircon (Spencer et al., 2019). This is not surprising given detrital zircon are sourced from diverse magmatic systems, with both mantle and supracrustal components. Time constraints for the change in average zircon $\delta^{18}O$ are from Spencer et al. (2019). Note that the solid black line shows the arithmetic mean of sediment-derived igneous zircon excluding samples 18IM14A and 18IM21C (reversely colored symbols; see Appendix 4.2 for detailed discussion of reasons for the exclusion of these two samples). Solid white line shows moving average of $\delta^{18}O$ for detrital zircon data (Spencer et al., 2019). The change in average zircon $\delta^{18}O$ is coeval with the Great Oxygenation Event (GOE), the timing of which is indicated by vertical blue line (rapid oxygenation) according to Luo et al. (2016), and by wider blue bar (oscillatory oxygenation) according to Gumsley et al. (2017), and a shift in average $\Delta^{17}O$ (defined as $\delta^{17}O$-0.5305*$\delta^{18}O$ [‰]) of shales as shown in (b). Shale triple-oxygen isotope data are from Bindeman et al. (2018). Results of statistical step-change analysis (Pettitt test) shown as solid black line in B) are from Spencer et al. (2019)

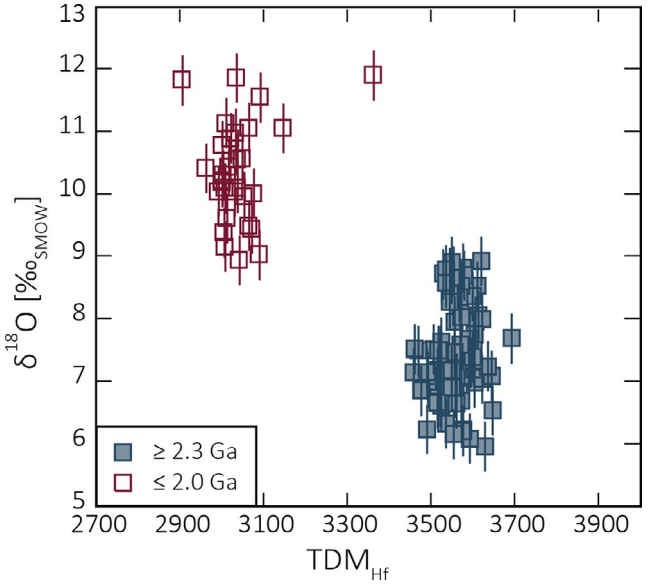

FIGURE 5 Depleted mantle model age (TDM_{Hf}) versus $\delta^{18}O$ of single grain analyses ($n = 154$) of igneous zircon from sediment-derived granitoids. Uncertainties are shown at two sigma level. Samples are colour-coded by crystallization age (i.e. ≥2.3 Ga, *n*= samples; ≤2.0 Ga, *n*= samples). TDM_{Hf} were calculated using the isotopic estimates of the depleted mantle from Vervoort et al. (2018), a ^{176}Lu decay constant of $1.867*10^{-11}$ $year^{-1}$ (Söderlund et al., 2004), and assuming an initial $^{176}Lu/^{177}Hf$ ratio of 0.01 (upper continental crust). While the absolute values calculated for TDM_{Hf} are highly sensitive to the assumed initial $^{176}Lu/^{177}Hf$ ratio, the relative differences of TDM_{Hf} are not affected. There is no correlation between depletion of radiogenic ^{176}Hf (leading to older TDM_{Hf} and lower εHf) and increasing $\delta^{18}O$ in the individual groups (i.e., the post-2.0 Ga and pre-2.3 Ga granitoids) indicating that enhanced crustal reworking alone did not cause the increase in $\delta^{18}O$

4 | DISCUSSION

4.1 | A Palaeoproterozoic increase in zircon $\delta^{18}O$ in sediment-derived melts

Our results taken together with the data from Dan et al. (2012), Marschall et al. (2010), and Mikkola et al. (2011) demonstrate a ~ 3.5‰ increase in average zircon $\delta^{18}O$ from 6.7‰ pre-2.3 Ga ($n = 16$) to 10.1‰ post-2.0 Ga ($n = 5$) in sediment-derived granitoids (Figure 4). Two samples (18IM14A, 18IM21C) are omitted from the calculation of the post-2.0 Ga zircon $\delta^{18}O$ average, as petrographic and geochemical evidence suggest that the zircon O isotope ratios may not be of primary magmatic origin or may have been inherited from an igneous source (see Appendix A). Our results are in accord with previous studies on detrital and igneous zircon demonstrating an increase in average $\delta^{18}O$ across the Archean-Proterozoic boundary (Spencer et al., 2019; Valley et al., 2005).

4.2 | Decoupled O and Hf isotopic signatures

The recycling of older crustal material leads to lower εHf values and older depleted mantle model ages (TDM_{Hf}) for zircon from melts that assimilated such material as compared to zircon (of the same age) from more juvenile melts (Hawkesworth & Kemp, 2006). The granitoids analysed in this study show no correlation between radiogenic ^{176}Hf depletion (older TDM_{Hf}) and high $\delta^{18}O$ in zircon (Figure 5). Younger TDM_{Hf} in the post-2.0 Ga granitoids indicate on average shorter crustal residence times of the precursors of these rocks as compared to the pre-2.3 Ga granitoids (Vervoort & Blichert-Toft, 1999). The lack of a correlation between older TDM_{Hf} and increasing $\delta^{18}O$ in the NCC granitoids is in accord with a previous study on detrital zircon that demonstrated decoupled behaviour of zircon $\delta^{18}O$ and TDM_{Hf} (Spencer et al., 2019). This feature has been interpreted as an indication that enhanced crustal reworking alone cannot account for the rise in zircon $\delta^{18}O$ (Spencer et al., 2019). This interpretation is supported by the timing of the ~2.35 Ga (Spencer et al., 2019) zircon $\delta^{18}O$ increase, that predates the ~1.9–1.8 Ga assembly of Nuna (Bleeker, 2003), and instead falls into a period characterized by a global lull in tectonomagmatic activity (Condie et al., 2009; Spencer et al., 2018).

4.3 | Changes in sediment composition as a driver for the zircon $\delta^{18}O$ increase

If enhanced crustal recycling is unable to account for the Paleoproterozoic increase in zircon $\delta^{18}O$, the explanation of the data presented here necessitates an increase in $\delta^{18}O$ in recycled material. It has been suggested that an increased clay-component in sedimentary rocks and subsequent incorporation into sediment melts could have driven the increase in zircon $\delta^{18}O$ (e.g., Payne et al., 2015). Clay-rich sediments and sediment melts tend to have higher Rb/Sr and Rb/Ba ratios than clay-poor ones (Sylvester, 1998). The NCC granitoids show Rb/Sr and Rb/Ba ratios that fall within the low end of Rb/Sr and Rb/Ba ratios reported for Archean to Phanerozoic sediment-derived granites elsewhere (Bucholz & Spencer, 2019; Sylvester, 1998), suggesting that the sediment-derived granitoids studied here may derive from the partial melting of relatively clay-poor sources (Sylvester, 1998). Rb/Ba and Rb/Sr ratios only provide a first order assessment of the maturity of the sedimentary source (i.e., clay-content) of sediment-derived melts as these ratios are also controlled by the melting reaction, and may be affected by secondary processes (Ennis et al., 2000; Harris & Inger, 1992) (see Appendix A for details). Importantly, however, neither the results of this study nor global datasets of sediments (Condie, 1993) and sediment-derived granitoids (Bucholz & Spencer, 2019) show evidence for a systematic increase in clay-component associated with the increase in zircon $\delta^{18}O$ (Figure 3), suggesting that sediment clay content was not a dominant control on the O isotope composition of these melts.

4.4 | The emergence of continents and its repercussion on sediment $\delta^{18}O$

Based on these results, we suggest that a change in the O isotopic composition of supracrustal material available for recycling

was the likely driver of the observed Paleoproterozoic change in average zircon $\delta^{18}O$. Sediments are the dominant high-$\delta^{18}O$ reservoir on Earth with shales comprising the largest fraction (Veizer & Mackenzie, 2003). The average $\delta^{18}O$ of non-glacial shales increases from ~10‰ in the Archean to ~13‰ in the Paleoproterozoic (Bindeman, 2020). The increase in shale $\delta^{18}O$ through time can be attributed to a variety of causes, including the onset of a modern hydrological cycle due to the subaerial emergence of continents (Bindeman et al., 2018), progressive recycling of sediments (Windley, 1995), a decrease in ocean temperature (Knauth & Lowe, 2003) or a decreasing contribution of hydrothermal clays to shales (Knauth & Lowe, 2003). In addition, aggressive chemical weathering under a CO_2-rich pre-GOE atmosphere may have stripped sediments of feldspar, the component required to form high-$\delta^{18}O$ authigenic clays (Lowe & Tice, 2004; Savin & Epstein, 1970). Furthermore, it has been suggested that increased freeboard led to the formation of Paleoproterozoic high-$\delta^{18}O$ shales that upon subsequent recycling caused an increase in zircon $\delta^{18}O$ (Payne et al., 2015; Spencer et al., 2019). Sedimentary reservoirs other than shales (e.g., silicic and carbonate oozes) also show a general increase in $\delta^{18}O$ across the Archean-Proterozoic boundary (Bindeman, 2020), and potentially contribute to increasing $\delta^{18}O$ in sediment-derived melts. However, based on their triple-oxygen isotope geochemistry, shales have been proposed to be the dominant assimilant or source of post-Archean sediment-derived granites (Bindeman, 2020). Intriguingly, the increase of zircon $\delta^{18}O$ in sediment-derived melts is coeval with a change in the triple-oxygen isotope composition of shales between 2.43 and 2.31 Ga, which is reasonably linked with the rapid emergence of large subaerial landmasses and associated changes in continental weathering pattern (Bindeman, 2020; Bindeman et al., 2018). The emergence of continents could have supported authigenesis in marine Al-rich sediments derived from the erosion of elevated continental crust (Hazen et al., 2013) causing an increase in shale $\delta^{18}O$ (Savin & Epstein, 1970). Paleoproterozoic atmospheric oxygenation may have further supported the rise in average $\delta^{18}O$ of shales through enhanced and diversified clay production as a consequence of oxidative subaerial weathering (Hazen et al., 2013). An increase of continental freeboard during the early Paleoproterozoic Era is consistent with a shift from predominantly submarine to predominantly subaerial large igneous province volcanism (Kump & Barley, 2007). The lifespan of sedimentary basins ranges from <1 Myr to >100 Myr (Woodcock, 2004). Hence, the compositional response of sediment melts to the increase in sediment $\delta^{18}O$ may be retarded due to the lag time between deposition and recycling. The timing of the $\delta^{18}O$ changes in shales (between 2.43 and 2.31 Ga; Bindeman, 2020) and detrital zircon (~2.35 Ga; Spencer et al., 2019) indicate a lag time of <100 Myr between these two records. Importantly, the <2.0 Ga granitoids of this study are interpreted to have <2.2–2.0 Ga sedimentary precursors, deposited well after (>100 Myr) the emergence of continents and the concomitant change in shale triple-oxygen isotope composition (Bindeman, 2020).

4.5 | Concluding remarks

The results of this study imply that the Paleoproterozoic widespread emergence of continents above sea-level and concomitant formation of high-^{18}O shales left an imprint on the composition of sediment melts (recorded by zircon $\delta^{18}O$). The coeval rise of atmospheric O_2 imply a potential link between continental emergence and atmospheric oxygenation, perhaps related to diminished submarine volcanism (Gaillard et al., 2011; Kump & Barley, 2007), or an increased supply of nutrients for photosynthetic microbes from emergent crust into the ocean (Hao et al., 2020).

4.6 | Statement of significance

The results of this study show that Paleoproterozoic secular change in O isotope composition of global sediment melts is caused by the widespread emergence of continents above sea-level. The implication is that the emergence of continents was coeval with the first significant build-up of O_2 in the atmosphere. Therefore, this study thus not only enhances our understanding of planetary crustal evolution, but importantly also demonstrates a potential trigger for a boost in oxygenic photosynthesis. Previous work on the secular evolution of crustal O isotopes has been based on detrital zircon, ultimately derived from a wide variety of magmatic sources including multicycle material. In contrast, this study focuses on magmatic zircon whose source can be precisely constrained (that is a direct melt of a sedimentary source). This sampling approach allows greater fidelity in interpretation of geochemical changes through time.

ACKNOWLEDGEMENTS

We thank two anonymous reviewers for their constructive comments and Klaus Mezger for editorial handling. Analytical work at the Guangzhou Institute of Geochemistry was supported by the open fund from the State Key Laboratory of Isotope Geochemistry, GIGCAS (SKLabIG-KF-18-04). The Centre for Microscopy, Characterisation & Analysis, University of Western Australia, is funded by the University, State and Commonwealth Governments. Analytical work in the John de Laeter Centre, Western Australia was enabled by AuScope (auscope.org.au) and the Australian Government via the National Collaborative Research Infrastructure Strategy (NCRIS), and funding from the Australian Research Council LIEF program (LE150100013).

CONFLICT OF INTEREST

No conflict of interest has been declared by the authors.

DATA AVAILABILITY STATEMENT

The data that support the findings of this study are available in the supplementary material of this article.

ORCID

Janne Liebmann https://orcid.org/0000-0002-0739-3148
Christopher L. Kirkland https://orcid.org/0000-0003-3367-8961

REFERENCES

Baertschi, P. (1976). Absolute 18O content of standard mean ocean water. *Earth and Planetary Science Letters*, *31*, 341–344. https://doi.org/10.1016/0012-821X(76)90115-1

Bindeman, I. N. 2020. Triple oxygen isotopes in evolving continental crust, granites, and clastic sediments. *Reviews in Mineralogy and Geochemistry*, *86*, https://doi.org/10.2138/rmg.2020.86.X

Bindeman, I. N., Zakharov, D. O., Palandri, J., Greber, N. D., Dauphas, N., Retallack, G. J., Hofmann, A., Lackey, J. S., Bekker, A., & Data, E. (2018). Rapid emergence of subaerial landmasses and onset of a modern hydrologic cycle 2.5 billion years ago. *Nature*, *557*, 545–548. https://doi.org/10.1038/s41586-018-0131-1

Bleeker, W. (2003). The late Archean record: A puzzle in ca. 35 pieces. *Lithos*, *71*, 99–134. https://doi.org/10.1016/j.lithos.2003.07.003

Bucholz, C. E., & Spencer, C. J. (2019). Strongly peraluminous granites across the Archean-Proterozoic transition. *Journal of Petrology*, *60*(7), 1299–1348. https://doi.org/10.1093/petrology/egz033

Chappell, B. W., & White, A. J. R. (1992). I- and S-type granites in the Lachlan Fold Belt. *Earth and Environmental Science Transactions of the Royal Society of Edinburgh*, *83*, 1–26. https://doi.org/10.1017/S0263593300007720

Condie, K. C. (1993). Chemical composition and evolution of the upper continental crust: Contrasting results from surface samples and shales. *Chemical Geology*, *104*, 1–37. https://doi.org/10.1016/0009-2541(93)90140-E

Condie, K. C. (2018). A planet in transition: The onset of plate tectonics on Earth between 3 and 2 Ga? *Geoscience Frontiers*, *9*, 51–60. https://doi.org/10.1016/j.gsf.2016.09.001

Condie, K. C., O'Neill, C., & Aster, R. C. (2009). Evidence and implications for a widespread magmatic shutdown for 250 My on Earth. *Earth and Planetary Science Letters*, *282*, 294–298. https://doi.org/10.1016/j.epsl.2009.03.033

Craig, H. (1961). Standard for reporting concentrations of deuterium and oxygen-18 in natural waters. *Science*, *133*, 1833–1834. https://doi.org/10.1126/science.133.3467.1833

Dan, W., Li, X., Guo, J., Liu, Y., & Wang, X. (2012). Integrated in situ zircon U-Pb age and Hf–O isotopes for the Helanshan khondalites in North China Craton: Juvenile crustal materials deposited in active or passive continental margin? *Precambrian Research*, *222–223*, 143–158. https://doi.org/10.1016/j.precamres.2011.07.016

Dan, W., Li, X.-H., Wang, Q., Wang, X.-C., Liu, Y., & Wyman, D. A. (2014). Paleoproterozoic S-type granites in the Helanshan Complex, Khondalite Belt, North China Craton: Implications for rapid sediment recycling during slab break-off. *Precambrian Research*, *254*, 59–72. https://doi.org/10.1016/j.precamres.2014.07.024

Eiler, J. M. (2001). Oxygen Isotope Variations of Basaltic Lavas and Upper Mantle Rocks. In J. W. Valley, & D. R. Cole (Ed.), *Stable Isotope Geochemistry. Reviews in Mineralogy and Geochemistry* (pp. 319–364). Mineralogical Society of America/Geochemical Society.

Ennis, D., Dunbar, N., Campbell, A., & Chapin, C. (2000). The effects of K-metasomatism on the mineralogy and geochemistry of silicic ignimbrites near Socorro. *New Mexico: Chemical Geology*, *167*, 285–312. https://doi.org/10.1016/S0009-2541(99)00223-5

Flament, N., Coltice, N., & Rey, P. F. (2013). The evolution of the 87Sr/86Sr of marine carbonates does not constrain continental growth. *Precambrian Research*, *229*, 177–188. https://doi.org/10.1016/j.precamres.2011.10.009

Frost, B. R., & Frost, C. D. (2008). A Geochemical Classification for Feldspathic Igneous Rocks. *Journal of Petrology*, *49*, 1955–1969. https://doi.org/10.1093/petrology/egn054

Gaillard, F., Scaillet, B., & Arndt, N. T. (2011). Atmospheric oxygenation caused by a change in volcanic degassing pressure. *Nature*, *478*, 229–232. https://doi.org/10.1038/nature10460

Gumsley, A. P., Chamberlain, K. R., Bleeker, W., Söderlund, U., de Kock, M. O., Larsson, E. R., & Bekker, A. (2017). Timing and tempo of the Great Oxidation Event. *Proceedings of the National Academy of Sciences*, *114*, 1811–1816. https://doi.org/10.1073/pnas.1608824114

Hao, J., Knoll, A. H., Huang, F., Hazen, R. M., & Daniel, I. (2020). Cycling phosphorus on the Archean Earth: Part I. *Continental Weathering and Riverine Transport of Phosphorus: Geochimica Et Cosmochimica Acta*, *273*, 70–84. https://doi.org/10.1016/j.gca.2020.01.027

Harris, N. B. W., & Inger, S. (1992). Trace element modelling of pelite-derived granites. *Contributions to Mineralogy and Petrology*, *110*, 46–56. https://doi.org/10.1007/BF00310881

Hawkesworth, C. J., & Kemp, A. I. S. (2006). Using hafnium and oxygen isotopes in zircons to unravel the record of crustal evolution. *Chemical Geology*, *226*, 144–162. https://doi.org/10.1016/j.chemgeo.2005.09.018

Hazen, R. M., Sverjensky, D. A., Azzolini, D., Bish, D. L., Elmore, S. C., Hinnov, L., & Milliken, R. E. (2013). Clay Mineral Evolution. *American Mineralogist*, *98*, 2007–2029. https://doi.org/10.2138/am.2013.4425

Hintze, J. L., & Nelson, R. D. (1998). Violin plots: A box plot-density trace synergism. *The American Statistician*, *52*, 181–184. https://doi.org/10.1080/00031305.1998.10480559

Hollis, J. A., Van Kranendonk, M. J., Cross, A. J., Kirkland, C. L., Armstrong, R. A., & Allen, C. M. (2014). Low δ18O zircon grains in the Neoarchean Rum Jungle Complex, northern Australia: An indicator of emergent continental crust. *Lithosphere*, *6*, 17–25. https://doi.org/10.1130/L296.1

Kirkland, C. L., Whitehouse, M. J., Pease, V., & Van Kranendonk, M. (2010). Oxygen Isotopes in Detrital Zircons: Insight into Crustal Recycling during the Evolution of the Greenland Shield. *Lithosphere*, *2*, 3–12. https://doi.org/10.1130/L80.1

Knauth, L. P., & Lowe, D. R. (2003). High Archean climatic temperature inferred from oxygen isotope geochemistry of cherts in the 3.5 Ga Swaziland Supergroup. *South Africa: Geological Society of America Bulletin*, *115*, 566–580. https://doi.org/10.1130/0016-7606(2003)115<0566:HACTIF>2.0.CO;2

Kump, L. R., & Barley, M. E. (2007). Increased subaerial volcanism and the rise of atmospheric oxygen 2.5 billion years ago. *Nature*, *448*, 1033–1036. https://doi.org/10.1038/nature06058

Lowe, D. R., & Tice, M. M. (2004). Geologic evidence for Archean atmospheric and climatic evolution: Fluctuating levels of CO2, CH4, and O2 with an overriding tectonic control. *Geology*, *32*, 493–496. https://doi.org/10.1130/G20342.1

Luo, G., Ono, S., Beukes, N. J., Wang, D. T., Xie, S., & Summons, R. E. (2016). Rapid oxygenation of Earth's atmosphere 2.33 billion years ago. *Science Advances*, *2*(5), e1600134. doi: https://doi.org/10.1126/sciadv.1600134

Marschall, H. R., Hawkesworth, C. J., Storey, C. D., Dhuime, B., Leat, P. T., Meyer, H.-P., & Tamm-Buckle, S. (2010). The Annandagstoppane Granite, East Antarctica: Evidence for Archaean Intracrustal Recycling in the Kaapvaal-Grunehogna Craton from Zircon O and Hf Isotopes. *Journal of Petrology*, *51*, 2277–2301. https://doi.org/10.1093/petrology/egq057

Mikkola, P., Huhma, H., Heilimo, E., & Whitehouse, M. (2011). Archean crustal evolution of the Suomussalmi district as part of the Kianta Complex, Karelia: Constraints from geochemistry and isotopes of granitoids. *Lithos*, *125*, 287–307. https://doi.org/10.1016/j.lithos.2011.02.012

O'Neill, C., Lenardic, A., Weller, M., Moresi, L., Quenette, S., & Zhang, S. (2016). A window for plate tectonics in terrestrial planet evolution? *Physics of the Earth and Planetary Interiors*, *255*, 80–92. https://doi.org/10.1016/j.pepi.2016.04.002

Page, F. Z., Fu, B., Kita, N. T., Fournelle, J., Spicuzza, M. J., Schulze, D. J., Viljoen, F., Basei, M. A. S., & Valley, J. W. (2007). Zircons from kimberlite: New insights from oxygen isotopes, trace elements, and Ti in zircon thermometry. *Geochimica Et Cosmochimica Acta*, *71*, 3887–3903. https://doi.org/10.1016/j.gca.2007.04.031

Payne, J. L., Hand, M., Pearson, N. J., Barovich, K. M., & Mcinerney, D. J. (2015). Crustal thickening and clay: Controls on O isotope variation in global magmatism and siliciclastic sedimentary rocks. *Earth and Planetary Science Letters*, *412*, 70–76. https://doi.org/10.1016/j.epsl.2014.12.037

Savin, S. M., & Epstein, S. (1970). The oxygen and hydrogen isotope geochemistry of clay minerals. *Geochimica Et Cosmochimica Acta*, *34*, 25–42. https://doi.org/10.1016/0016-7037(70)90149-3

Söderlund, U., Patchett, P. J., Vervoort, J. D., & Isachsen, C. E. (2004). The 176Lu decay constant determined by Lu–Hf and U-Pb isotope systematics of Precambrian mafic intrusions. *Earth and Planetary Science Letters*, *219*, 311–324. https://doi.org/10.1016/S0012-821X(04)00012-3

Spencer, C. J., Cawood, P. A., Hawkesworth, C. J., Raub, T. D., Prave, A. R., & Roberts, N. M. W. (2014). Proterozoic onset of crustal reworking and collisional tectonics: Reappraisal of the zircon oxygen isotope record. *Geology*, *42*, 451–454. https://doi.org/10.1130/G35363.1

Spencer, C. J., Murphy, J. B., Kirkland, C. L., & Liu, Y. (2018). Was the supercontinent cycle activated by a Palaeoproterozoic tectono-magmatic lull? *Nature Geoscience*, *11*, 97–101. https://doi.org/10.1038/s41561-017-0051-y

Spencer, C. J., Partin, C. A., Kirkland, C. L., Raub, T. D., Liebmann, J., & Stern, R. A. (2019). Paleoproterozoic increase in zircon δ18O driven by rapid emergence of continental crust. *Geochimica Et Cosmochimica Acta*, *257*, 16–25. https://doi.org/10.1016/j.gca.2019.04.016

Spencer, C. J., Roberts, N. M. W., & Santosh, M. (2017). Growth, destruction, and preservation of Earth's continental crust. *Earth-Science Reviews*, *172*, 87–106. https://doi.org/10.1016/j.earscirev.2017.07.013

Sylvester, P. J. (1998). Post-collisional Strongly Peraluminous Granites. *Lithos*, *45*, 29–44. https://doi.org/10.1016/S0024-4937(98)00024-3

Valley, J. W., Chiarenzelli, J. R., & McLelland, J. M. (1994). Oxygen isotope geochemistry of zircon. *Earth and Planetary Science Letters*, *126*, 187–206. https://doi.org/10.1016/0012-821X(94)90106-6

Valley, J. W., Lackey, J. S., Cavosie, A. J., Clechenko, C. C., Spicuzza, M. J., Basei, M. A. S., Bindeman, I. N., Ferreira, V. P., Sial, A. N., King, E. M., Peck, W. H., Sinha, A. K., & Wei, C. S. (2005). 4.4 billion years of crustal maturation: Oxygen isotope ratios of magmatic zircon. *Contributions to Mineralogy and Petrology*, *150*, 561–580. https://doi.org/10.1007/s00410-005-0025-8

Veizer, J., & Mackenzie, F. T.. (2003). Evolution of Sedimentary Rocks. In: *Treatise on Geochemistry* (pp. 369–407). : Elsevier Ltd.

Vervoort, J. D., & Blichert-Toft, J. (1999). Evolution of the depleted mantle: Hf isotope evidence from juvenile rocks through time. *Geochimica Et Cosmochimica Acta*, *63*, 533–556. https://doi.org/10.1016/S0016-7037(98)00274-9

Vervoort, J. D., Kemp, A. I., & Fisher, C. M.. (2018). Hf isotope constraints on evolution of the depleted mantle and growth of continental crust. In: *American Geophysical Union*, *Fall Meeting* 2018.

Wan, Y., Peng, P., Liu, S., Kröner, A., Guo, J., Dong, C., & Liu, D. (2018). Late Paleoproterozoic tectono-thermal event in the northwestern North China Craton: Evidence from U-Pb dating and O-Hf isotopic compositions of zircons from metasedimentary rocks north of Hohhot City. *Inner Mongolia*, *Northern China: Journal of Asian Earth Sciences*, *167*, 152–164. https://doi.org/10.1016/j.jseaes.2017.09.012

Wang, D., & Guo, J. (2017). Late Archean high-pressure pelitic granulites in the Yinshan Block, North China Craton. *Precambrian Research*, *303*, 251–267. https://doi.org/10.1016/j.precamres.2017.03.027

Windley, B. F. (1995). *The Evolving Continents*. Wiley & Sons.

Woodcock, N. H. (2004). Life Span and Fate of Basins. *Geology*, *32*, 685. https://doi.org/10.1130/G20598.1

Zhao, G., Wilde, S. A., Cawood, P. A., & Lu, L. (1999). Tectonothermal history of the basement rocks in the western zone of the North China Craton and its tectonic implications. *Tectonophysics*, *310*, 37–53. https://doi.org/10.1016/S0040-1951(99)00152-3

SUPPORTING INFORMATION

Additional supporting information may be found online in the Supporting Information section.

How to cite this article: Liebmann J, Spencer C, Kirkland CL, et al. Emergence of continents above sea-level influences sediment melt composition. *Terra Nova*. 2021;00:1–10. https://doi.org/10.1111/ter.12531